Steady-state cavitation modeling in an open source framework: Theory and applied cases

Lucian Hanimann, Luca Mangani, Ernesto Casartelli, Matthias Widmer

HAL Id: hal-01890070

https://hal.science/hal-01890070

Submitted on 8 Oct 2018

Steady-state cavitation modeling in an open source framework: Theory and applied cases

Lucian Hanimann[1]*, Luca Mangani[1], Ernesto Casartelli[1], Matthias Widmer[1]

Abstract

This paper deals with the steady state cavitation modeling and associated numerical challenges. Although cavitation is most often an unsteady phenomenon [1, 2] it is necessary to have a robust and reliable software able to represent the steady state (time averaged) flow patterns. Especially in the early design state it is mandatory to be able to predict the occurrence of cavitation without time consuming transient computations.

The authors will therefore give a short summary of the theory behind different cavitation models and their implementation into an in-house modified version of OpenFOAM®.

The main focus of the paper will then point out the integration of mixture type cavitation models into a pressure correction based steady-state solver. Different strategies have been tested and a stable formulation was found.

Keywords

Cavitation — Steady-State — CFD

[1]*Lucerne University of Applied Science and Arts, Lucerne, Switzerland*

Corresponding author: lucian.hanimann@hslu.ch

NOMENCLATURE

A_p	Matrix of Momentum Coefficients	
CC	Commercial Code	
d	Characteristic Length	$[m]$
f	Mass Fraction	
k	Turbulent Kinetic Energy	$[m^2 s^{-2}]$
k_l, k_p, k_v	Model Coefficients for Merkle Model	
n	Vapor bubble density	$[m^{-3}]$
p	Pressure	$[Pa]$
p_∞	Free Stream Pressure	$[Pa]$
R or S_α	Mass Exchange Rate	$[kg m^{-3} s^{-1}]$
$\dot{R}$	Bubble Growth Radius	$[m s^{-1}]$
R_b	Bubble Radius	$[m]$
r_e	Equivalent Radius	$[m]$
t	Time	$[s]$
t_∞	Free Stream Time Scale	$[s]$
u	Velocity	$[m s^{-1}]$
U_∞	Free Stream Velocity	$[m s^{-1}]$
V_{cell}	Cell Volume	$[m^3]$
∇	Gradient Operator	
$\nabla \cdot$	Divergence Operator	

Subscripts

c	Condensation
e	Evaporation
i	Phase Index (l or v)
l	Liquid
sat	Saturation
t	Turbulent
v	Vapor

Superscripts

$'$	Correction
$*$	Previous Solution

Greeks

α	Volume Fraction	
δ	Partial Derivative	
ϵ	Turbulent Dissipation	$[m^2 s^{-3}]$
γ or D_α	Effective Exchange Rate	$[kg m^{-1} s^{-1}]$
μ	Dynamic Viscosity	$[Pa s^{-1}]$
ρ	Density	$[kg m^3]$
σ	Cavitation Number	

Diacritic Marks

$^-$	Average

INTRODUCTION

In regions of strong acceleration the pressure has to drop to account for the increase in kinetic energy. If this pressure drop undergoes the saturation pressure, the phase changes. Such liquid-to-vapor phase-changes are usually related to temperature changes and therefore associated with evaporation. In this special case it is based on a pressure change and called cavitation.

The existence of cavitation is mostly undesired since it leads to vibrational fatigue, induced noise and increased erosion of the considered body [3, 4]. On the other hand it also rises an interesting field for improvements since it can drastically reduce the drag of a body [5, 6]. Several numerical studies have been conducted through the past years but still, the prediction of cavitation is a challenging task. Most often the inherent unsteady nature of the phenomena is tackled by time consuming transient simulation, although it may have a representative steady-state solution.

For industrial applications it is therefore necessary to enable steady-state prediction of the cavitation phenomena. This rises several challenges to the numerical procedure. Cavitation models are empirical or semi-analytical correlations, often based on the Rayleigh-Plesset model for bubble growth [7]. All these models have their constraints on the prediction of cavitation and investigation is needed on the global performance of these models.

Most of the available publications focus on the physics of the cavitation solver but less on the numerical challenges. For transient simulations, which is the general case for cavitation prediction, this may not be of great importance, since with sufficiently small time step, the numerical solution may converge anyway. However, this will lead to high computational costs which makes the procedure useless for everyday engineering applications. This could be circumvented by using steady state computations. To make this step, a deeper understanding and investigation of the numerics is needed.

Literature survey has shown that, although often used, little is described on the implementation of the published models. This is especially the case when the described model has to be ported from the theoretical test cases onto real turbomachinery applications. A stable, second order accurate implementation for 3D, viscous flows has to be found, applicable to systems with multiple frames of reference.

The present paper will therefore first recapitulate the very basic equations based on a consistent nomenclature and discuss some of the most often used models and their variations. Based on the experience gained during the literature survey and the validation, a toolbox will be presented. It should provide the reader with an overview about different models and modifications as well as enable to implement a reliable and robust numerical cavitation solver.

First the very basic model, the homogeneous equilibrium model, is introduced. In a next step the mass exchange between the phases has to be addressed. Here, the phase fraction equation is introduced and the difficulties encountered during literature review commented and clarified.

In a next step, the SIMPLE-based pressure correction equation in its non-zero velocity divergence form is introduced. Having now the complete set of Navier-Stokes equations and the additional fraction equation, the models for the transfer rate are introduced.

We will then continue with some of the best known models and discuss some of the modifications, suggested by other authors during the years.

The validation will be carried out by two well known test cases. For the analysis of stability and performance a first simple test case was chosen, the blunt-body test case of Rouse and McKnown. To prove the applicability and stability of the implemented procedure a marine propeller, distributed at the "Second International Symposium on Marine Propulsors 2011" (smp'11) [8], was chosen.

1. METHODS

In this section we will introduce step-by-step the final cavitation solver, starting with the homogeneous equilibrium model, introducing the phase fraction and modified Navier-Stokes equations and finally discussing the phase exchange models and their modifications.

1.1 Homogeneous equilibrium model

The homogeneous equilibrium model states that the velocity, temperature and pressure between the two phases are equal. This assumption is based on the belief that momentum, energy and mass transfer are fast enough to reach equilibrium.

Mixture density (Eq. 1) and viscosities (Eq. 2) are therefore introduced in the Navier-Stokes equations (Momentum and Continuity).

$$\bar{\rho} = \alpha_v \rho_v + \alpha_l \rho_l \tag{1}$$

$$\bar{\mu} = \alpha_v \mu_v + \alpha_l \mu_l \tag{2}$$

Where α_v and α_l are the vapor and liquid volume fraction respectively.

1.2 Phase Fraction Equation

Since only one set of NS-equations is solved, the contribution of the phase change is accounted by empirical or semi-analytical equations and an additional transport equation for the phase fraction. The general transport equation can either be stated in form of mass (Eq. 3) or volume fraction (Eq. 5).

$$\frac{\delta \bar{\rho} f_i}{\delta t} + \nabla \cdot (\bar{\rho} \underline{u} f_i) = \nabla \cdot (\gamma \nabla f_i) + R_i \tag{3}$$

With the definition of the mass fraction as in Eq. 4, the transport equation can be rewritten in terms of volume fraction (Eq. 5).

$$f_i = \frac{\rho_i}{\bar{\rho}} \alpha_i \tag{4}$$

$$\frac{\delta \rho_i \alpha_i}{\delta t} + \nabla \cdot (\rho_i \underline{u} \alpha_i) = \nabla \cdot (\gamma \nabla \frac{\rho_i}{\bar{\rho}} \alpha_i) + R_i \tag{5}$$

Where R_i is the mass exchange rate and generally expressed as $R_v = Re - Rc$ if stated for the vapor fraction. Therefore $R_v = -R_l$.

γ is usually known as the effective exchange rate coefficient. Although often presented in literature [9, 10, 11] it was difficult to find a description of this contribution and was only found in one single paper so far [12]. According to these authors it is the "diffusive mass flux of vapor penetrating across the cluster of an equivalent radius r_e into the surrounding fluid". This is a well known approach to increase the spreading rate of a transported quantity.

The equation in [12] was given as shown in Eq. 6.

$$\frac{\delta \rho_v \alpha_v}{\delta t} + \nabla \cdot (\rho_v \underline{u} \alpha_v) - \nabla \cdot D_\alpha \nabla \alpha = S_\alpha \tag{6}$$

With the effective exchange coefficient:

$$D_\alpha = \rho \dot{R} r_e \tag{7}$$

The equivalent radius is defined as:

$$r_e = \left[\frac{3 \alpha_v V_{cell}}{4\pi} \right]^{\frac{1}{3}} \tag{8}$$

r_e describes the radius inside which also surrounding cells should be influenced by the phase change mass exchange.

$\dot{R}$ is the bubble growth radius and can be derived from the Rayleigh-Plesset equation for bubble dynamics. The resulting equation, Eq. 9, is a first order approximation after dropping the non-linear acceleration term, the surface tension and viscous contribution from the original formulation.

$$\dot{R} = sign(p_{sat} - p) \sqrt{\frac{2}{3} \frac{p_{sat} - p}{\rho_l}} \tag{9}$$

Compared to the original formulation stated by Singhal et al. [10] in (Eq. 3) this would imply that Eq. 10 holds.

$$\nabla \cdot D_\alpha \nabla \alpha_v = \nabla \cdot \gamma \nabla \frac{\alpha_v}{\bar{\rho}}$$
$$D_\alpha \nabla \alpha_v = \rho_v \gamma \nabla \frac{\alpha_v}{\bar{\rho}}$$
$$D_\alpha \nabla \alpha_v = \rho_v \gamma \left(\alpha_v \nabla \bar{\rho}^{-1} + \bar{\rho}^{-1} \nabla \alpha_v \right) \tag{10}$$

It is clear that there must be a difference between the implementations described in literature and it is not clear which implementation is correct or represents the reality in a better way. Since most authors did not account for this effective mass exchange coefficient it was decided to neglect this diffusion-like contribution in the implemented model.

The final form of the phase fraction equation for steady state computations was implemented for the liquid phase given in Eq. 12:

$$\nabla \cdot u_l \alpha_l = \frac{R_l}{\rho_l} \tag{11}$$

$$\nabla \cdot u_l \alpha_l = \frac{R_c - R_e}{\rho_l} \tag{12}$$

With ϕ representing the conserved volume flux through the cell faces including Rhie-Chow correction.

It is important to note that the semi-analytical models for the mass exchange are very often dependent on the phase fractions as well. This implicit dependency of the mass exchange-rate on the vapor fraction has to be integrated in the coefficient matrix to obtain a robust numerical implementation. Not only may it improve the solution procedure of the linear system itself but also enables an update of the effective exchange rate during inner iterations. In order to achieve a robustness which allows steady state computations this is a mayor contribution to a successful implementation.

1.3 Pressure-correction equation

For the update of the pressure a non-conservative, so called non-zero velocity divergence equation was used to formulate a basis for the derivation of a pressure-correction equation. Summing up the two volume-fraction equations we can derive Eq. 13 for the velocity divergence. This formulation was suggested by [13], also based on experience of [14, 15].

$$\nabla \underline{u} = \left(\frac{1}{\rho_v} - \frac{1}{\rho_l} \right) R_v \tag{13}$$

Using the definition of pressure correction equation for the SIMPLE algorithm as given in Eq. 15

$$u'_j = -\frac{1}{A_p} \frac{\delta p'}{\delta x_j} \tag{14}$$

$$\frac{\delta u'_j}{\delta x_j} = \frac{\delta}{\delta x_j} \left[-\frac{1}{A_p} \frac{\delta p'}{\delta x_j} \right] \tag{15}$$

with the definition of u'_j as

$$u'_j = u_j - u^\star_j \tag{16}$$

with the $\star$ referring to previous iteration solution of the iterative numerical procedure.

Using Eq. 13, Eq. 15 can be rewritten consistently as Eq. 17:

$$\frac{\delta}{\delta x_j} \left[-\frac{1}{A_p} \frac{\delta p'}{\delta x_j} \right] = \left(\frac{1}{\rho_v} - \frac{1}{\rho_l} \right) R_v - \frac{\delta u^\star_j}{\delta x_j} \tag{17}$$

The mass exchange contribution is, however, a relatively big term which is added to the source of the equation. It is therefore necessary to use a first order Taylor series as suggested by [16] to partially treat the source term as an implicit matrix contribution.

$$R|_{new} = R|_{old} + \frac{\delta}{\delta p} R|_{old} p' \tag{18}$$

1.4 Cavitation Models

Four different cavitation models are considered. The Kunz, Merkle and Schnerr-Sauer model are already available in OpenFOAM. The Zwart model was then added since it is one of the standard models for commercial codes.

1.4.1 Kunz et al. 2000 [17]

The model by Kunz was developed for sheet and super cavitating flows. Sheet cavitation is known to have a gas-liquid interface which is nearly in dynamic equilibrium and pressure and velocity over the interface do not vary heavily [17].

The transition from vapor to liquid R_e was modeled as linear to pressure and liquid fraction. For the liquid-to-vapor change R_c a simplified Ginzburg-Landau relationship was used.

$$R_e = \frac{C_{dest}\rho_v\alpha_l \, min\,[0, p - p_{Sat}]}{\rho_l \frac{U_\infty^2}{2} t_\infty}$$

$$R_c = \frac{C_{prod}\rho_v\alpha_l^2(1 - \alpha_l)}{t_\infty} \qquad (19)$$

The coefficients used hereafter are:

$$C_{dest} = 1000 \qquad C_{prod} = 1000 \qquad (20)$$

U_∞ is the free stream velocity and t_∞ the free stream time scale usually defined as d/U_∞ with d as the characteristic length scale e.g. the body diameter.

1.4.2 Merkle et al. 2006 [18]

The model by Merkle et al. is an improved version of the model by Kunz et al. However, it uses a boundedness criterion (f) for the evaporation and condensation rate to ensure numerical stability.

$$R_e = k_v \frac{\rho_v\alpha_l}{t_\infty} \underbrace{min\left[1, max\left(\frac{p_{Sat} - p}{k_p p_v}, 0\right)\right]}_{f}$$

$$R_c = k_l \frac{\rho_v\alpha_v}{t_\infty} \underbrace{min\left[1, max\left(\frac{p - p_{Sat}}{k_p p_v}, 0\right)\right]}_{f} \qquad (21)$$

1.4.3 Schnerr-Sauer-Yuan 2001 [13]

This model is based on the approach that the mixture contains a large number of spherical bubbles. The mass exchange rate is then based on a simplified model for bubble growth based on the Rayleigh-Plesset equation. It should therefore account for non-equilibrium effects.

$$R_e = \frac{\rho_v\rho_l}{\bar{\rho}}\alpha_v(1 - \alpha_v)\frac{3}{R_b}\sqrt{\frac{2}{3}\frac{p_{Sat} - p}{\rho_l}}$$

$$R_c = \frac{\rho_v\rho_l}{\bar{\rho}}\alpha_v(1 - \alpha_v)\frac{3}{R_b}\sqrt{\frac{2}{3}\frac{p - p_{Sat}}{\rho_l}} \qquad (22)$$

With R_b being the bubble radius given as:

$$R_b = \left(\frac{\alpha_v}{1 - \alpha_v}\frac{3}{4\pi n}\right)^{\frac{1}{3}} \qquad (23)$$

The only constant which has to be determined is the number of vapor bubbles per volume of liquid (n). As stated by [13], a value of $1.5 10^{14} nuclei/m_{Water}^3$ yields good agreement with experimental observation of [19].

1.4.4 Zwart et al. 2004 [20]

Like the Schnerr-Sauer model, the Zwart model is based on a simplified Rayleigh-Plesset equation to account for non-equilibrium effects. In order to better account for the interaction of the cavitation bubbles, the nucleation site density must decrease as the vapor volume fraction increases.

Therefore, the original r_v was replaced by $r_{nuc}(1 - r_v)$

- $R_B = 10^{-6}m$ (Nucleation site radius)

- $r_{nuc} = 5 \cdot 10^{-4}$

- $F_{vap} = 50$

- $F_{cond} = 0.01$

$$R_e = F_{vap}\frac{3r_{nuc}(1 - \alpha_v)}{R_b}\rho_v\sqrt{\frac{2}{3}\frac{p_{Sat} - p}{\rho_l}}$$

$$R_c = F_{cond}\frac{3\alpha_v}{R_b}\rho_v\sqrt{\frac{2}{3}\frac{p - p_{Sat}}{\rho_l}} \qquad (24)$$

1.5 Modifications

Several modifications of the cavitation models have been introduced during the last years. Mainly to better account for the turbulence effects on the vapor-liquid interface. In the next two sections we will discuss two of the best known modifications.

1.5.1 Eddy-Viscosity

According to the literature [20], it is observed that standard turbulence models fail to properly predict the oscillating behavior of the flow close to the liquid-vapor interface.

Reboud et al. [21] suggested a modified formulation of the turbulent eddy viscosity.

The definition of the eddy viscosity is given in Eq. 25.

$$\mu_t = \bar{\rho}C_\mu\frac{k^2}{\epsilon} \qquad (25)$$

The modified formulation uses an adaption of the mixture density $\bar{\rho}$ in order to reduce the turbulent viscosity in the mixture region. This implementation showed to improve the cavitation prediction and was therefore adapted in the implemented turbulence model.

$$\mu_t = f(\rho)C_\mu\frac{k^2}{\epsilon} \qquad (26)$$

$$f(\rho) = \rho_v + \left(\frac{\rho_v - \bar{\rho}}{\rho_v - \rho_l}\right)^n(\rho_l - \rho_v) \qquad (27)$$

Another possibility to account for the turbulent fluctuations is Singhal's pressure modification, which he claimed to be more robust.

1.5.2 Singhal et al. 2002 [10]

Although not implemented in the here proposed library, Singhal et al. 2002 introduced a modification which may be useful in cavitation prediction. Their model for cavitation prediction is called the "Full Cavitation Model" since it should account for:

- Formation and transport of vapor bubbles

- Turbulent fluctuation of pressure and velocity

- Magnitude of non-condensible gases

The following equations describe the mass transfer rate:

$$R_e = C_e \frac{V_{Ch}}{\sigma} \rho_l \rho_v \sqrt{\frac{2}{3} \frac{p_{Sat} - p}{\rho_l}} \frac{\rho_v}{\bar{\rho}} (1 - \alpha_v)$$

$$R_c = C_c \frac{V_{Ch}}{\sigma} \rho_l \rho_v \sqrt{\frac{2}{3} \frac{p - p_{Sat}}{\rho_l}} \frac{\rho_v}{\bar{\rho}} \alpha_v \qquad (28)$$

V_{Ch} represents the velocity, which reflects the effect of the local relative velocity between liquid and vapor. Usually $\sqrt{k}$ is used.

In order to better represent the turbulent pressure fluctuations they suggested the following equation for these contributions:

$$p'_t = 0.39 \bar{\rho} k \qquad (29)$$

This is further used to modify the local saturation pressure of the flow as

$$p_{Sat}|_{new} = p_{Sat} + p'_t / 2 \qquad (30)$$

This, however, is a rather arbitrary modification, and it has to be taken care what pressure is used in the momentum equation. The Reynolds averaging of the NS-equations introduces a pressure like contribution of the turbulent fluctuations,which is often substituted by a new pressure for the gradient expression in the NS-equations for stability reasons and therefore dropped from the turbulence equations. This is not the case for the implemented solver and an additional modification of the pressure due to turbulent fluctuations was considered misleading.

2. TEST CASE 1: ROUSE AND MCNOWN

In the 1940s, Rouse and McNown conducted a series of experimental analysis of various simple body shapes to investigate the cavitation phenomenon. A closed-loop variable pressure water tunnel was build and the results were presented in 1948 in [22].

These test cases are very well known in literature [23, 24, 25] and therefore chosen for the validation of the present implementation.

Out of this extensive experimental data the blunt-body case was chosen and investigated for three different cavitation numbers $\sigma \in [0.3 \ 0.4 \ 0.5]$ to prove the generality of the models and numerical implementations.

The definition of the cavitation number is given as:

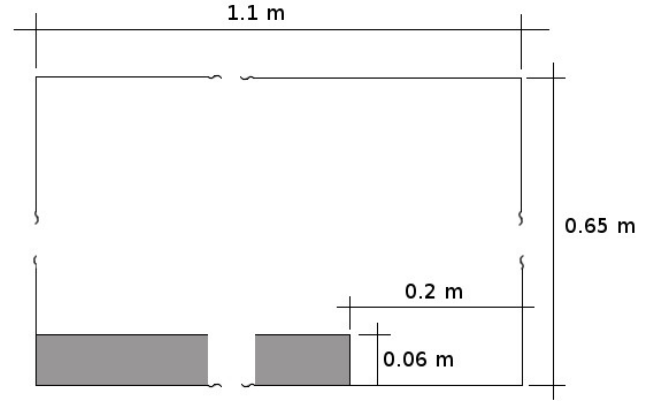$$\sigma = 2 \frac{p_\infty - p_{Sat}}{\rho_l U_\infty^2} \qquad (31)$$

Figure 1. Blunt Body Domain

2.1 Mesh and boundary conditions
The overall domain bounding box is given in Fig. 1.

The operating conditions are only dependent on Reynolds and cavitation number. The Reynolds number in the experiment is $1.36 \cdot 10^5$, based on the body diameter as characteristic length scale.

- $L_{char} = 0.1359 m$

- $u_\infty = 0.8926 \frac{m}{s}$

- $p_\infty = 101325 Pa$

2.2 Results
Steady state solutions were achieved and presented in Fig. 2,3 and 4. It can be stated that the model by Kunz et al. performed best. All the other models led to an over prediction of the recirculation region. Moreover, the Merkle model was only sufficiently stable for steady state computations by ad hoc modifications. They are therefore not presented since not trustworthy enough.

The above mentioned modification on the saturation pressure, given by Singhal et al. [10] in order to improve the influence of pressure fluctuations extremely lowered the robustness of the solution procedure and compared to the measurement results, did not improve the capabilities of the solver.

3. TEST CASE 2: PPTC

The Potsdam Propeller Testcase (PPTC) [26] was used during the Second International Symposium on Marine Propulsors 2011 (smp'11) [8] as a reference case for cavitation model validation. It is based on the model propeller VP1304 and tested at the SVA Potsdam in a closed loop cavitation tunnel, see Fig. 5. Testsection indicated in red.

The original test section has a length of 2600mm and a cross section of 600x600mm. The propeller is located 570mm
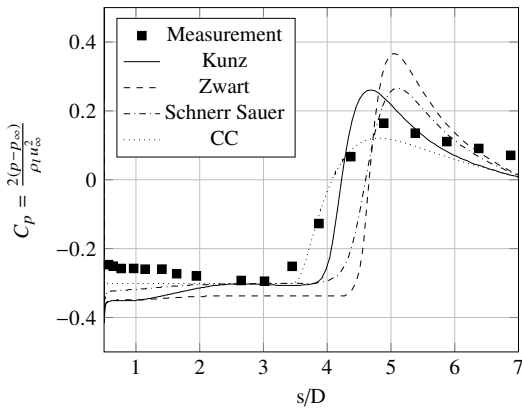
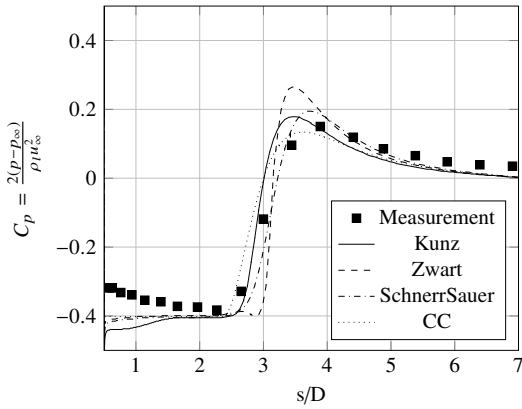**Figure 2.** Pressure coefficient for $\sigma = 0.3$
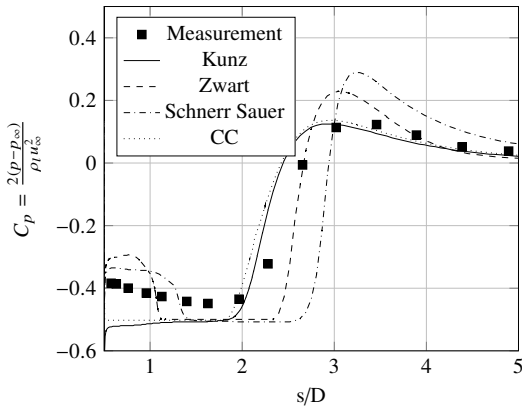

Figure 3. Pressure coefficient for $\sigma = 0.4$

Figure 4. Pressure coefficient for $\sigma = 0.5$

Figure 5. Cavitation Tunnel
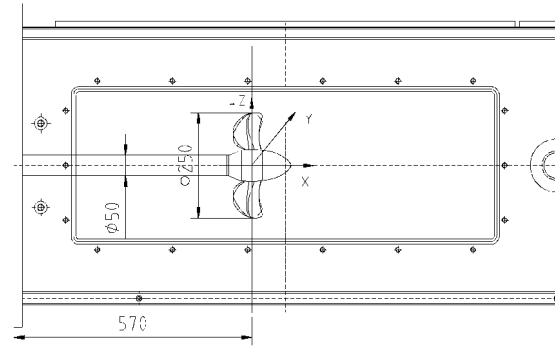
Figure 6. Propeller Configuration

Thermophysical properties:

- Density of water as liquid: $997.4 \frac{kg}{m^3}$

- Density of water as vapor: $0.02095 \frac{kg}{m^3}$

- Kinematic viscosity water as liquid: $0.9280 \cdot 10^-6 \frac{m^2}{s}$

- Kinematic viscosity water as vapor: $468.62 \cdot 10^-6 \frac{m^2}{s}$

- Saturation pressure $p_{Sat} = 2818$

Propeller data:

- Rotational Speed $n = 24.987[1/s]$

- Propeller diameter $D = 0.25[m]$

The idea of the experiment is to obtain thrust identity for the non-cavitating propeller. The cavitation models are then activated, affecting on the thrust of the propeller.

Turbulence modeling is based on the SST model [27]. For the inlet boundary conditions a turbulent intensity of 5% and an eddy viscosity ratio of 10 was assumed. Based on the results from the first test case, the Kunz model was chosen for the cavitation simulation.

The reason for this test case comes with two arguments. First, there are a lot of participants of smp'11 for comparison. Additionally, there is a serious lack of publicly available test

down of the inlet and has a diameter of 250mm, see Fig. 6.

For the numerical computation, the rectangular cross section was replaced with a circular one with the same crosssectional area. This adaption of the geometry was a suggestion of the smp'11 organizers. Operating conditions can be determined by advance coefficient and cavitation number. All water properties are at $23.2°C$.
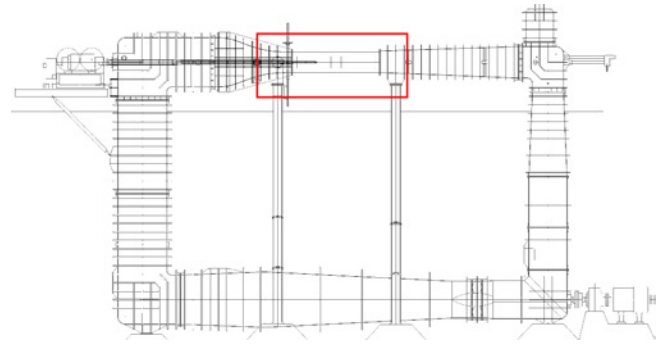
cases. There would be another test case, which would even provide better measurement data for comparison [28]. Sadly the available geometrical data is of poor quality, which would raise questions on the validity of the simulation.

3.1 Evaluation

As for the smp'11 the evaluation is done by comparing the numerical results against experiments. Two different views were printed for each test case for qualitative comparison.

- Case 2.3.1 and 2.3.2: In flow direction on suction side (SS) and side view on suction side (SVSS)

- Case 2.3.3: In flow direction on pressure side (PS) and side view on pressure side (SVPS)

In order to judge the quality of the cavitation prediction, three different images were generated with a value fraction of vapor of 0.2, 0.5 and 0.8.
In this paper, the effect of the threshold value will be shown based the first case 2.3.1.

3.2 Case 2.3.1

Case 2.3.1 is in off-design conditions and the operating conditions are given by:

- Advance coefficient $J = \frac{U}{nD} = 1.019$

- Cavitation number $\sigma_n = \frac{2(p-p_{Sat})}{\rho_l(nD)^2} = 2.024$

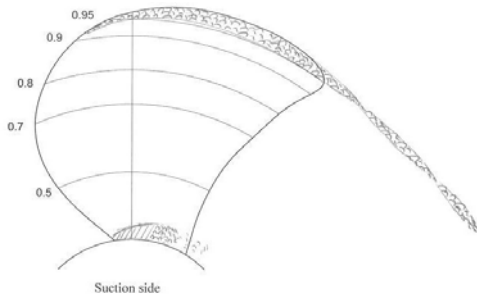- Thrust coefficient $K_T = \frac{T}{\rho_l n^2 D^4} = 0.387$

Figure 7. Measurement Visualization

As can be seen from Fig. 8, a major difference is present in the leading edge region. While for the experimental data no cavitation occurs, the numerical solution predicts a thin layer of vapor. Comparing to the results of the competitors of smp'11, this was predicted by all contributors using sophisticated CFD software, except for the team "VOITH-Comet".
Since the occurrence of cavitation requires the pressure to drop below the saturation pressure, this difference can not be related to the cavitation model, but to a difference in the prediction of the pressure field. Although this can be influenced by e.g. turbulence model and/or numerical schemes,
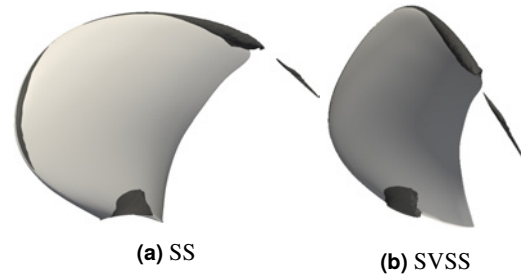

(a) SS   **(b)** SVSS

Figure 8. Kunz, Void Fraction 0.8, High Resolution

it is more likely to be a difference between the experimental setup and the boundary conditions given by the organizers, e.g. the reduction to a circular cross section. This statement is confirmed by the fact that the difference in these regions can be observed throughout the other competitors.
The remaining flow features are comparable to the competitors of the smp'11. While most competitors did not resolve a tip vortex, a small portion was resolved, after refinement of the mesh and the use of a curvature correction model, see [29]. However, some of the competitors of smp'11 predicted a really stable tip vortex which matches the experimental results better.
As for the leading edge vapor layer, it has to be considered that cavitation demands the presence of regions below vapor pressure. Therefore, in the opinion of the authors, the difference can not be completely attributed of the cavitation model. It would require more investigation in turbulence modeling and mesh requirements to better predict the pressure gradients in these regions.
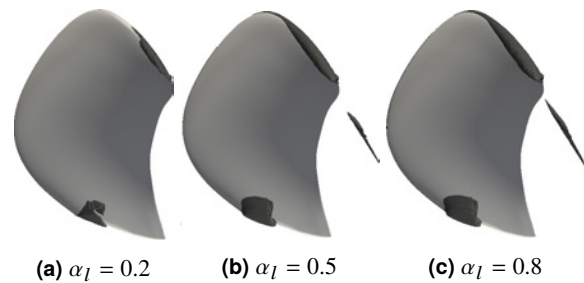

(a) $\alpha_l = 0.2$ **(b)** $\alpha_l = 0.5$ **(c)** $\alpha_l = 0.8$

Figure 9. Comparison of the influence of void fraction

Fig. 9 shows a comparison of the cavitation region for different void fractions. Compared to the results of smp'11 this is in close agreement with the best achieved solutions. Qualitative comparison is shown in Tab. 1.
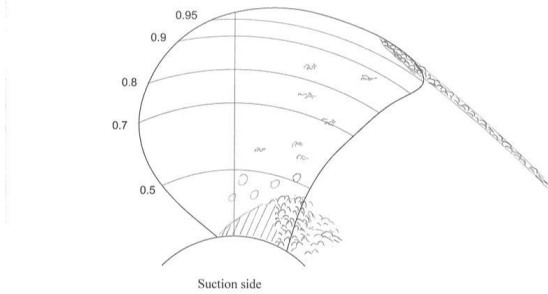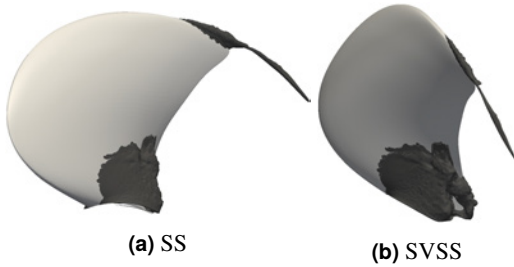
3.3 Case 2.3.2

Case 2.3.2 is at design conditions and the operating conditions are given by:

- Advance coefficient $J = \frac{U}{nD} = 1.269$

- Cavitation number $\sigma_n = \frac{2(p-p_{Sat})}{\rho_l(nD)^2} = 1.424$

Table 1. Thrust coefficient for case 2.3.1

	Cavitating Case	Non-cavitating case
Measurement	0.387	0.373
Simulation	0.387	0.379
Error %	-	1.7

Table 2. Thrust coefficient for case 2.3.2

	Non-cavitating Case	Cavitating case
Measurement	0.245	0.2064
Simulation	0.245	0.2050
Error %	-	-0.68

- Thrust coefficient $K_T = \frac{T}{\rho_l n^2 D^4} = 0.245$

Figure 10. Measurement Visualization

(a) SS   **(b)** SVSS

Figure 11. Kunz, Void Fraction 0.8, High Resolution

As can be seen in Fig. 11 the tip vortex as well as the cavitation region close to the hub were predicted in agreement with the measured results, as well as with results of smp'11. A comparison of thrust coefficient for this case is given in Tab. 2.

3.4 Case 2.3.3
Case 2.3.3 is again in off-design conditions and the operating conditions are given by:
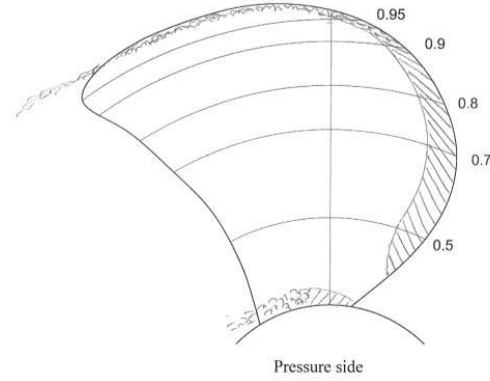
- Advance coefficient $J = \frac{U}{nD} = 1.408$

- Cavitation number $\sigma_n = \frac{2(p - p_{Sat})}{\rho_l (nD)^2} = 2$

- Thrust coefficient $K_T = \frac{T}{\rho_l n^2 D^4} = 0.167$

For this case, pressure side cavitation should occur.
 As for all the results of smp'11, the tip vortex could not be resolved. Although generally well defined, the geometrical data was missing information about the tip topology. Discontinuities in the model were present and due to a lack of

Figure 12. Measurement Visualization

(a) PS   **(b)** SVPS
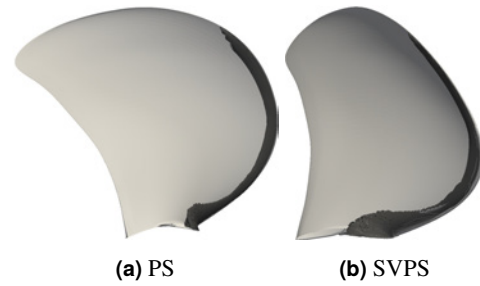
Figure 13. Kunz, Void Fraction 0.8, High Resolution

additional information, these regions had to be modified by the users best knowledge. Even if these modifications were very small and only affected the tip region of the blade, this will have an influence on the development of the tip vortex. The values for thrust coefficient can be found in table 3.

3.5 Overall qualitative comparison, Thrust coefficient
The overall comparison of the thrust coefficient shows good agreement with measurement results and is among the best predictions of all results of smp'11 as can be seen from Tab. 4. Not only is the thrust reduction prediction close to experimental values, but it is also the most consistent for the different operating points.

4. CONCLUSIONS

In this paper a review of existing models for cavitation analysis was presented. Based on this review a detailed description of the equations was given and suggestions for the numeri-

Table 3. Thrust coefficient for case 2.3.3

	Cavitating Case	Non-cavitating case
Measurement	0.167	0.1362
Simulation	0.166	0.1374
Error %	-	0.87

Table 4. Results of smp'11 including the steady-state solutions

	Error %		
Results	2.3.1	2.3.2	2.3.3
Berg-Procal	0.94		
Cradle-SC/Tetra	0.67	-3.59	1.32
CSSRC-Fluent	0.4	-6.01	-3.08
INSEAN-PFC	-4.16	12.89	18.21
SSPA-Fluent	4.16	-0.68	5.73
TUHH-FreSCO+	2.82		5.73
UniGenua-Panel	5.29	14.78	1.17
UniTries-StarCCM	1.53	-1.41	-4.11
UniTries-CFX(FCM)	0.4	-1.65	-4.55
UniTries-CFX(Kunz)	0.67	-1.74	-2.35
UniTries-CFX(Zwart)	0.13	-5.04	-2.35
VOITH-Comet	3.41	1.79	11.09
VTT-FinFlo	3.62	-2.13	4.26
HSLU-OF	**1.7**	**-0.68**	**0.87**

cal treatment of different contributions shown. Based on this information it should allow a programmer to implement a stable numerical procedure for the prediction of steady-state cavitation phenomena. Various modifications of the original cavitation models have been tested and it was pointed out that some harm the stability in an intolerable manner or are even physically questionable.

An overview about the most up-to-date models is presented and it is noticed that, although presented and published, some of the models are not fully described, e.g. the effective exchange coefficient. Here deeper investigation or clarification by the authors would be needed.

The implemented models were finally validated on a well known simple test case, based on the experiments of Rouse and McNown. It could be shown, that of all the models, the one by Kunz performed best, while theoretically more sophisticated models overpredicted the cavitating region.

In terms of stability, it had to be concluded that the model of Merkle showed major convergence difficulties and was therefore not further investigated.

Applicability to real turbomachinery applications could be

shown by the PPTC marine propeller. Due to a lack of experimental data, only a visual comparison was made. However, it was shown that the regions of cavitation are in good agreement with the experiments and are consistent with the results of most of the participants of smp'11.

The differences on the suction and pressure side, away of the tip region, are believed to be a result of inappropriate boundary conditions, given by the smp'11 organizers. The occurrence of cavitation in this region is only dependent on the mean flow field and a difference would state that even without cavitation the numerical solution would differ from the measurement. Since the difference is observed through all participants, the discrepancy can probably not be related to the cavitation model.

Considering the tip region, it can be observed that a much stronger vortex is present in the measurement than in the numerical analysis. This, however, is the case for almost all the candidates of smp'11. A curvature correction model was implemented and the mesh was refined in order to better resolve the pressure gradient. Considering tip vortex prediction and the accompanied cavitation occurrence it has to be stated that further investigation in turbulence modeling is needed.

Comparing the global results, given by the thrust reduction, the prediction was in good agreement with the measurement data. Not only was it among the best predictions of the results of smp'11, but also the most consistent for the different operating points.

ACKNOWLEDGMENTS

REFERENCES

[1] Benoit Pouffary. Numerical Modelling of Cavitation. Technical report, DTIC Document, 2006.

[2] Rickard E Bensow and Göran Bark. Simulating cavitating flows with LES in openfoam. 2010.

[3] Mario Peron, Etienne Parkinson, Lothar Geppert, and Thomas Staubli. Importance of jet quality on Pelton efficiency and cavitation. In *Proceedings of the IGHEM, International Conference on Hydraulic Efficiency Measurements, Milan, Italy, Sept*, pages 3–6, 2008.

[4] P Gruber, D Roos, C Müller, and T Staubli. Detection of damaging cavitation states by means of ultrasonic signal parameter patterns. In *WIMRC (3rd International Cavitation Forum), Warwick, UK*, 2011.

[5] Eduard Amromin, Jim Kopriva, Roger EA Arndt, and Martin Wosnik. Hydrofoil drag reduction by partial cavi-

tation. *Journal of Fluids Engineering*, 128(5):931–936, 2006.

[6] Eduard Amromin, Gabor Karafiath, and Bryson Metcalf. Ship drag reduction by air bottom ventilated cavitation in calm water and in waves. *Journal of Ship Research*, 55(3):196–207, 2011.

[7] Lord Rayleigh. Viii. On the pressure developed in a liquid during the collapse of a spherical cavity. *The London, Edinburgh, and Dublin Philosophical Magazine and Journal of Science*, 34(200):94–98, 1917.

[8] International Symposium on Marine Propulsors. `http://www.marinepropulsors.com/`. Accessed: 2015-12-01.

[9] Mahesh M Athavale, HY Li, YU Jiang, and Ashok K Singhal. Application of the full cavitation model to pumps and inducers. *International Journal of Rotating Machinery*, 8(1):45–56, 2002.

[10] Ashok K Singhal, Mahesh M Athavale, Huiying Li, and Yu Jiang. Mathematical basis and validation of the full cavitation model. *Journal of fluids engineering*, 124(3):617–624, 2002.

[11] G Palau-Salvador, P Gonzalez Altozano, and J Arviza-Valverde. Numerical modeling of cavitating flows for simple geometries using FLUENT V6. 1. *Spanish Journal of Agricultural Research*, 5(4):460–469, 2007.

[12] Vedanth Srinivasan, Abraham J Salazar, and Kozo Saito. Numerical simulation of cavitation dynamics using a cavitation-induced-momentum-defect (CIMD) correction approach. *Applied Mathematical Modelling*, 33(3):1529–1559, 2009.

[13] Weixing Yuan, Jürgen Sauer, and Günter H Schnerr. Modeling and computation of unsteady cavitation flows in injection nozzles. *Mécanique & industries*, 2(5):383–394, 2001.

[14] J Sauer and GH Schnerr. Unsteady cavitating flow–a new cavitation model based on a modified front capturing method and bubble dynamics. In *Proceedings of 2000 ASME Fluid Engineering Summer Conference*, pages 11–15, 2000.

[15] D.B. Spalding. A method for computing steady and unsteady flows possessing discontinuities of density. In *CHAM Report*, volume 910/2, 1974.

[16] J Sauer. Instationär Kavitierende Strömungen-ein neues Modell, basierend auf Front Capturing (vof) und Blasendynamik, 2000. *Fakultät für Maschinenbau Universität Karlsruhe, Germany*.

[17] Robert F Kunz, David A Boger, David R Stinebring, Thomas S Chyczewski, Jules W Lindau, Howard J Gibeling, Sankaran Venkateswaran, and TR Govindan. A preconditioned Navier–Stokes method for two-phase flows with application to cavitation prediction. *Computers & Fluids*, 29(8):849–875, 2000.

[18] CL Merkle and DV Li. Sankaran, Multi-Disciplinary Computational Analysis in Propulsion. AIAA-2006-4374, 42nd AIAA/ASME/SAE/ASEE Joint Propulsion Conference, Sacramento. USA, 2006.

[19] P Roosen, O Unruh, and M Behmann. Untersuchung und Modellierung des transienten Verhaltens von Kavitationserscheinungen bei ein-und mehrkomponentigen Kraftstoffen in schnell durchströmten Düsen. *Report of the Institute for Technical Thermodynamics, RWTH Aachen, Germany*, 1996.

[20] Philip J Zwart, Andrew G Gerber, and Thabet Belamri. A two-phase flow model for predicting cavitation dynamics. In *Proceedings of the fifth international conference on multiphase flow, Yokohama, Japan*, 2004.

[21] Olivier Coutier-Delgosha, R Fortes-Patella, and Jean-Luc Reboud. Evaluation of the turbulence model influence on the numerical simulations of unsteady cavitation. *Journal of Fluids Engineering*, 125(1):38–45, 2003.

[22] Hunter Rouse and John S McNown. Cavitation and pressure distribution: head forms at zero angle of yaw. 1948.

[23] Robert F Kunz, Jules W Lindau, Michael L Billet, and David R Stinebring. *Multiphase CFD modeling of developed and supercavitating flows*. Defense Technical Information Center, 2001.

[24] Y Saito, I Nakamori, and T Ikohagi. Numerical analysis of unsteady vaporous cavitating flow around a hydrofoil. In *Fifth International Symposium on Cavitation, Osaka, Japan, Nov*, pages 1–4, 2003.

[25] Robert F Kunz, David A Boger, Thomas S Chyczewski, D Stinebring, H Gibeling, and TR Govindan. Multi-phase CFD analysis of natural and ventilated cavitation about submerged bodies. In *Proceedings of FEDSM*, volume 99, 1999.

[26] Schiffbau-Versuchsanstalt Potsdam. `http://www.sva-potsdam.de/pptc_data.html`. Accessed: 2015-12-01.

[27] Florian R Menter. Two-equation eddy-viscosity turbulence models for engineering applications. *AIAA journal*, 32(8):1598–1605, 1994.

[28] G Calcagno, F Di Felice, M Felli, S Franchi, F Pereira, and F Salvatore. The INSEAN E779a propeller test case: a database for CFD validation. In *Proceedings of the Marnet-CFD Final Workshop*, 2003.

[29] Pavel E Smirnov and Florian R Menter. Sensitization of the SST turbulence model to rotation and curvature by applying the Spalart–Shur correction term. *Journal of Turbomachinery*, 131(4):041010, 2009.